Compressed sensing of monostatic and multistatic SAR

Ivana Stojanovic, *Member, IEEE,* Mujdat Cetin, *Senior Member, IEEE,* and W. Clem Karl, *Senior Member, IEEE*

***Abstract*—In this paper we study the impact of compressed data collections from a SAR sensor on reconstruction quality of a scene of interest. Different monostatic and multistatic SAR measurement configurations produce different Fourier sampling patterns. These patterns reflect different spectral and spatial diversity trade-offs that must be made during task planning. Compressed sensing theory argues that the mutual coherence of the measurement probes is related to the reconstruction performance of sparse domains. With this motivation we propose a closely related $t_{\%}$-average mutual coherence parameter as a sensing configuration quality parameter and examine its relationship to the reconstruction behavior of various monostatic and ultra-narrow band multistatic configurations. We investigate how this easily computed metric is related to SAR reconstruction quality.**

I. Introduction

Synthetic aperture radar (SAR) is a remote sensing system capable of producing high-resolution imagery of target scenes independent of time of day, distance, and weather. Conventional SARs are monostatic, with collocated transmit and receive antenna elements. These SAR sensors coherently process multiple, sequential observations of a scene under the assumption that the scene is static. Imaging resolution is determined by the bandwidth of the transmitted signals and the size of the synthesized antenna. Greater resolution requires wider bandwidths and larger aspect angles obtained from a longer baseline observation interval. An alternative approach is based on multistatic configurations, wherein spatially dispersed transmitters and receivers sense the scene. Such configurations provide the opportunity for spatial as well as frequency diversity and offer potential advantages in flexible sensor planning, sensing time reduction, and jamming robustness.

To exploit the promise of multistatic sensing, robust methods of reconstructing imagery obtained from general multistatic configurations are needed, as well as tools to understand and evaluate the performance of various sensor configuration choices in a straightforward, tractable manner. Recently the area known as compressed sensing (CS) [1], [2] has received much attention in the signal processing field. CS seeks to acquire as few measurements as possible about an unknown signal, and given these measurements, reconstruct the signal either exactly or with provably small probability of error. The reconstruction methods used in CS are related to sparsity-constrained, non-quadratic regularization. Signal reconstruction accuracy is shown to be related to the mutual coherence of the corresponding measurement operator [3], [4]. Furthermore, the CS literature has demonstrated accurate signal reconstructions from measurement of extremely few, but randomly chosen Fourier samples of a signal [2], [5]. Since SAR can be viewed as obtaining samples of the spatial Fourier transform of the scattering field [6], these results suggest interesting opportunities for SAR sensing.

The use of sparsity constrained reconstructions for SAR image formation was first presented in [7], although not within the compressed sensing framework. More recently, there have been several applications of compressed sensing ideas to radar [8], [9], [10], [11]. The authors in [8] accurately reconstruct a small number of targets on a time-frequency plane by transmitting a sufficiently incoherent pulse and employing the techniques of compressed sensing. The authors in [10] propose the use of chirp pulses and pseudo-random sequences for compressed sensing with imaging radars. A compressed sensing technique for a synthetic aperture radar is also discussed in [9], where the authors obtain measurements by random subsampling of a regular aspect-frequency grid in $\mathbf{k}$-space. A SAR compressed sensing with reduced number of probes was first discussed in [12] and [13].

In contrast to the previous work, we extend compressed sensing treatments to the multistatic scenario and propose a $t_{\%}$-mutual coherence parameter of the measurement operator as a simple measure of sensing configuration quality. Within this framework, we examine different monostatic and ultra-narrowband multistatic configurations, which trade off frequency and geometric diversity. We show how the $t_{\%}$-mutual coherence of the measurement operator is affected by the number of transmitting probes as well as by the number of measurements, and we investigate and demonstrate how this simple metric is related to reconstruction quality.

II. Multistatic SAR signal model

We consider a general multistatic system with spatially distributed transmit and receive antenna elements within a cone positioned at the center of a scene of interest.The scene of interest is modeled by a set of point scatterers reflecting impinging electromagnetic waves isotropically to all receivers within the cone. We introduce a coordinate system with the origin in the center of the area of interest and, for simplicity, model the scene as two dimensional (Fig. 1). The relative size of the scene is assumed to be small compared to distances from the origin of the coordinate system to all transmitters and receivers, such that transmit and receive angles would change negligibly if the coordinate origin moved to any point in the scene. Furthermore, we neglect signal propagation attenuation.

The complex signal received by the l-th receiver, located at $\mathbf{x}_l = [x_l, y_l]^T$, for the narrow-band excitation from the

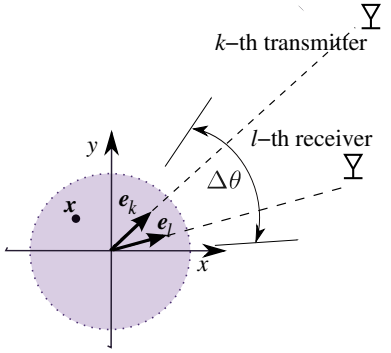

Fig. 1. Geometry of the kl-th transmit-receive pair with respect to the scene of interest. All transmit and receive pairs are restricted to lie within a cone of the angular extent $\Delta\theta$.

k-th transmitter, located at $\mathbf{x}_k = [x_k, y_k]^T$, reflected from a point scatterer at the spatial location $\mathbf{x} = [x, y]^T$ is given by $r_{kl}(t) = s(\mathbf{x})\, \gamma_k\left(t - \tau_{kl}(\mathbf{x})\right)$, where $s(\mathbf{x})$ is the reflectivity of the scatterer, $\gamma_k(t)$ is the transmitted waveform from the k-th transmitter, and $\tau_{kl}(\mathbf{x})$ is the propagation delay from the transmitter to the scatterer and back from the scatterer to the receiver. The overall received signal from the entire ground patch with radius L is then modeled as a superposition of the returns from all the scattering centers. For narrow-band waveforms, defined by $\gamma_k(t) = \tilde{\gamma}_k(t)e^{j\omega_k t}$, where $\tilde{\gamma}_k(t)$ is a low-pass, slowly varying signal and ω_k the carrier frequency, the received signal is given by:

$$r_{kl}(t) = \int_{\|\mathbf{x}\| \leq L} s(\mathbf{x}) e^{j\omega_k (t - \tau_{kl}(\mathbf{x}))}\, \tilde{\gamma}_k\left(t - \tau_{kl}(\mathbf{x})\right)\, d\mathbf{x}. \quad (1)$$

In the far-field case, when $\|\mathbf{x}\| \ll \|\mathbf{x}_k\|$, $\|\mathbf{x}\| \ll \|\mathbf{x}_l\|$, and $\omega_k/c\|\mathbf{x}\|^2 \ll \|\mathbf{x}_k\|$, $\omega_k/c\|\mathbf{x}\|^2 \ll \|\mathbf{x}_l\|$, we can use the first order Taylor series expansion to approximate the propagation delay $\tau_{kl}(\mathbf{x})$ as:

$$\tau_{kl}(\mathbf{x}) = \frac{1}{c}\left(\|\mathbf{x}_k - \mathbf{x}\| + \|\mathbf{x}_l - \mathbf{x}\|\right) \approx \tau_{kl}(\mathbf{0}) - \frac{1}{c}\mathbf{x}^T\mathbf{e}_{kl},$$

where $\tau_{kl}(\mathbf{0}) \doteq (\|\mathbf{x}_k\| + \|\mathbf{x}_l\|)/c$ is the known transmitter-origin-receiver propagation delay, and $\mathbf{e}_{kl} \doteq \mathbf{e}_k + \mathbf{e}_l$ is the kl-th transmit-receiver pair's bistatic range vector. The vectors $\mathbf{e}_k \doteq [\cos\phi_k, \sin\phi_k]^T$ and $\mathbf{e}_l \doteq [\cos\phi_l, \sin\phi_l]^T$ are unit vectors in the direction of the k-th transmitter and l-th receiver respectively.

The chirp signal is the most commonly used spotlight SAR pulse [6], given by $\gamma_k(t) = e^{j\alpha_k t^2} \cdot e^{j\omega_k t}, -\frac{\tau_c}{2} \leq t \leq \frac{\tau_c}{2}$ where ω_k is the center frequency and $2\alpha_k$ is the so-called chirp rate of the k-th transmit element. The narrow-band assumption is satisfied by choosing the chirp signal parameters such that $2\pi B_k/\omega_k \ll 1$. Ultra-narrow band waveforms are special cases of the chirp signal obtained by setting $\alpha_k = 0$.

We use a general transmitted chirp signal in (1), along with the far-field delay approximation, and apply typical demodulation and baseband processing [6], to obtain the following observed signal model:

$$r_{kl}(t) \approx \int_{\|\mathbf{x}\| < L} s(\mathbf{x}) e^{j\Omega_{kl}(t)\mathbf{x}^T\mathbf{e}_{kl}}\, d\mathbf{x}, \quad (2)$$

where $\Omega_{kl}(t) = \frac{1}{c}[\omega_k - 2\alpha_k(t - \tau_{kl}(\mathbf{x}_o))]$, depends on the frequency content of the transmitted waveform.

The received signal model for the monostatic configuration corresponds to collocated transmit-receiver pairs, and thus, is a special case of the multistatic model obtained by setting $\mathbf{x}_k = \mathbf{x}_l$.

III. Compressed sensing SAR

Compressed sensing enables reconstruction of sparse or compressible signals from a small set of linear, non-adaptive measurements, much smaller in size than required by the Nyquist-Shannon theorem [2], [1]. With high probability, accurate reconstructions can be obtained by sparsity-enforcing optimization techniques provided that the signal's sparsifying basis and the random measurement basis are sufficiently incoherent.

According to (2), SAR data represent Fourier $\mathbf{k}$-space measurements of the underlying spatial reflectivity field. Different monostatic and multistatic SAR measurement configurations produce different Fourier sampling patterns. These patterns reflect different spectral and spatial trade-offs that must be made during task planning. Compressed sensing theory argues that random Fourier measurements represent good projections for compressive sampling of point-like signals [2]. This suggests a natural application to the sparse aperture SAR sensing problem and opens a question of how different monostatic and multistatic SAR sensing configuration constraints influence reconstruction quality for fixed number of measurements. Furthermore, we are interested in a simple goodness measure that can predict configuration quality before sensing even takes place. Such a quality predictor would allow better task planning and resource utilization. From compressed sensing we know that the mutual coherence of the measurement probes is related to the worst case reconstruction performance of sparse domains [3], [4]. With this motivation we examine the relationship of the sensing geometry and a closely related parameter we term the $t_{\%}$-average mutual coherence, as this parameter is expected to provide a better measure of the average reconstruction quality than the mutual coherence which is a pessimistic measure.

In the following we first describe reduced data collections with non-conventional SAR $\mathbf{k}$-space sampling patters. Next, we describe the sparsity-enforcing reconstruction and define the $t_{\%}$-average mutual coherence parameter used for *a-priori* evaluation of such sensing configurations.

A. Sampling configurations

1) Monostatic SAR: One approach to reduced data collection is to directly reduce the number of transmitted probes with regular or random interrupts in the synthetic aperture. We consider several regular and random observation sampling patters within a fixed observation extent $\Delta\Theta$, coupled with regular and random frequency sampling within a desired chirp-signal bandwidth B. We do not constrain random aspect/frequency samples to fall on a regular rectangular grid. Fig. 2(a) illustrates the $\mathbf{k}$-space sampling pattern when both aspect and frequency are sampled regularly, and Fig. 2(b)

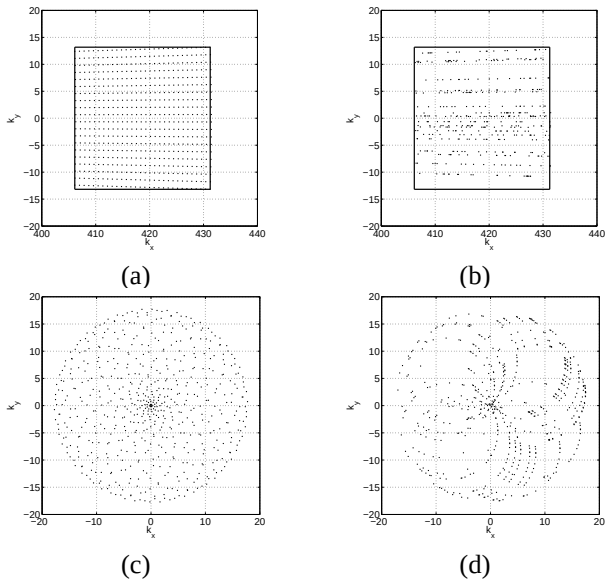

Fig. 2. (a), (b) Monostatic SAR **k**-space sampling patterns for a fixed **k**-space extent ($f_0 = 10$GHz, $B = 600$MHz, $\Delta\theta = 3.5\,\mathrm{deg}$). (c), (d) Multistatic **k**-space sampling patterns for circular, ultra-narrowband SAR operator, with $N_f = 1$, $N_{tx} = 20$ transmitters and $N_{rx} = 30$ receivers. (a) Regular aspect-frequency sampling. (b) Random aspect, random frequency sampling. (c) Regular transmitter-receiver aspect positioning. (d) Random transmitter, random receiver aspect positioning.

illustrates a realization of a **k**-space sampling pattern when both aspect and frequency are sampled randomly.

2) Multistatic SAR: Multistatic SAR offers the possibility of different **k**-space sampling patterns with trade-offs in temporal frequency and spatial transmit/receiver location diversity. In the monostatic case, the chirp signal bandwidth allowed for extended coverage of the **k**-space in the range direction. However, in the multistatic case, extended **k**-space coverage can also be achieved with ultra-narrowband signals provided there is spatial diversity of transmitter and receiver locations. Here, we consider a circular multistatic SAR with a continuous wave, ultra-narrowband signal transmission. For the general multistatic SAR, the total number of measurements is calculated as $M = N_{tx}N_{rx}N_f$, where N_{tx} is the number of transmitters/transmitted probes, N_{rx} is the number of receivers, and N_f is the number of frequency samples. In the case of the ultra-narrowband transmission we have $N_f = 1$ and different sampling patterns are achieved by varying transmitter and receiver angular locations. Figure 2(c) illustrates the **k**-space sampling pattern when both transmitter and receiver angular locations are sampled regularly, and Figure 2(d) illustrates a realization of **k**-space sampling when both transmitter and receiver locations are sampled randomly.

B. Sparse reconstruction

We consider image formation of target scenes consisting of a sparse set of point reflectors. The spatial reflectivity is reconstructed on a rectangular grid, resulting in the linear discrete-data SAR model:

$$\mathbf{r} = \tilde{\mathbf{\Phi}}\mathbf{s} + \mathbf{n},$$

where $\mathbf{s}$ is the unknown spatial reflectivity vector, and $\tilde{\mathbf{\Phi}}$ is derived by discretizing (2). The vector $\mathbf{r}$ represents the observed, thus known, set of return signals at all receivers across time. Its elements are indexed by the tuple (k, l, t_s), with t_s being the sampling times associated with the kl-th transmit-receive pair, and the spatial frequency $\Omega_{kl}(t)$ and aspect-vector samples $\mathbf{e}_{kl}$ are determined from the sampling configuration requirements.

Both the observed SAR data $\mathbf{r}$, and the underlying scattering field $\mathbf{s}$ are complex valued. In SAR applications reflectivity magnitudes are of primary interest. We apply sparsity-enforcing regularization directly on the magnitudes of the complex reflectivity field $\mathbf{s}$. In particular, we define the reduced data SAR reconstruction problem as:

$$\widehat{\mathbf{s}} = \quad \arg\min_{\mathbf{s}} \ \|\mathbf{s}\|_1^1 \quad \text{s.t.} \quad \|\mathbf{r} - \tilde{\mathbf{\Phi}}\mathbf{s}\|_2 \leq \sigma, \qquad (3)$$

where σ represents the regularization parameter and $\|\mathbf{s}\|_1^1 = \sum_i \sqrt{(\mathcal{R}(\mathbf{s})_i)^2 + (\mathcal{I}(\mathbf{s})_i)^2}$. We solve the optimization problem (3) using the software described in [14].

C. The t%-average mutual coherence

The mutual coherence of a measurement operator was discussed as a simple, but conservative measure of the ability of sparsity-enforcing reconstruction to accurately reconstruct a signal [3], [4]. In the case of complex $\tilde{\mathbf{\Phi}}$, the mutual coherence of a sensing geometry is defined as:

$$\mu(\tilde{\mathbf{\Phi}}) = \max_{i \neq j} g_{ij}, \qquad g_{ij} = \frac{| < \phi_i, \phi_j > |}{\|\phi_i\|_2 \|\phi_j\|_2}, i \neq j \qquad (4)$$

where ϕ_i is the i-th column of the matrix $\tilde{\mathbf{\Phi}}$, and the inner product is defined as $< \phi_i, \phi_j >= \phi_i^H \phi_j$. The i-th column vector ϕ_i can be viewed as a range-aspect 'steering vector' of a sensing geometry or a contribution of a scatterer at a specific spatial location to the received, phase history signal. The mutual coherence measures the worst case correlation between responses of two distinct spatially distributed reflectors. A less conservative measure connected to average reconstruction performance was proposed in [15] for compressed sensing projection optimization. The t-average mutual coherence was defined as the average value of the set $\{g_{ij} \mid g_{ij} > t\}$. In contrast to the t-average mutual coherence, we propose to use the $t_{\%}$-average mutual coherence as a measure more closely related to the average reconstruction performance of (3). We define the $t_{\%}$-average mutual coherence, $\mu_{t_{\%}}$, as follows. Let $\mathcal{E}_{t_{\%}}$ be the set of the $t_{\%}$ percent of the largest column cross-correlations g_{ij}. The $t_{\%}$-average mutual coherence is defined as:

$$\mu_{t_{\%}}(\tilde{\mathbf{\Phi}}) = \frac{\sum_{i \neq j} g_{ij} \mathcal{I}_{ij}(t_{\%})}{\sum_{i \neq j} \mathcal{I}_{ij}(t_{\%})}, \ \mathcal{I}_{ij}(t_{\%}) = \begin{cases} 1, & g_{ij} \in \mathcal{E}_{t_{\%}} \\ 0, & \text{otherwise.} \end{cases}$$

In other words, $\mu_{t_{\%}}(\tilde{\mathbf{\Phi}})$ measures an average cross-correlation value in a set of the $t_{\%}$ most similar column pairs. The parameter $t_{\%}$ should have a small value in order to accurately represent the tail of the column cross-correlation distribution. This measure is more robust to outliers, which can unfairly dominate the mutual coherence. A large value of $\mu_{t_{\%}}(\tilde{\mathbf{\Phi}})$ indicates a large number of similar columns of $\tilde{\mathbf{\Phi}}$ that can potentially confuse the reconstruction algorithm.

IV. Simulations

In this section we present simulation results averaged over 100 Monte Carlo runs. For regular sampling, we average over different ground truth scene realizations. In cases that involve random sampling we average over different SAR operator and ground scene realizations. For each realization of $\tilde{\mathbf{\Phi}}$ we measure the $t_{\%}$-average mutual coherence $\mu_{t_{\%}}(\tilde{\mathbf{\Phi}})$, for $t_{\%} = 0.5\%$, and display its average over all Monte Carlo runs. The ground truth scene consists of T randomly dispersed scatterers each with unit magnitude and random phase uniformly distributed in the range $[0, 2\pi]$.

Reconstruction performance is measured through the relative mean square error (RMSE), and the percentage of identified support. The RMSE is defined as RMSE $= E[\|\widehat{\mathbf{s}} - \mathbf{s}_0\|_2/\|\mathbf{s}_0\|_2]$, where $\mathbf{s}_0$ is the ground truth signal, $\widehat{\mathbf{s}}$ is its estimate from a reduced set of measurements, and $E[\cdot]$ stands for an empirical average over Monte Carlo runs. The percentage of identified support measures the percentage of the correctly identified support of the T largest components of the estimated signal.

1) Simulation results for monostatic CS SAR: We consider monostatic spotlight SAR imaging of a small ground patch of size $(D_x, D_y) = (10, 10)$m , when observed over a narrow-angle aspect cone of $\Delta\theta = 3.5\,\text{deg}$. The transmitted waveforms are chirp signals with $f_o = 10$GHz and $B = 600$MHz. The nominal range resolution is $\rho_x = \frac{c}{2B} = .25$m and the nominal cross-range resolution is $\rho_y = \frac{\lambda}{4\sin(\Delta\theta/2)} = .25$m. Assuming that the pixel spacing matches the nominal resolution, we seek to reconstruct a 40×40 pixel reflectivity image.

In Fig. 3 we show results when the ground scene consists of $T = 140$ randomly dispersed, non-zero, scatterers. The left column shows results at the fixed number of measurements $M = N_{tx}N_f = 600$ as we vary the number of transmitted probes N_{tx}. The right column shows results as a function of the number of measurements M for sensing configurations with equal number of frequency and aspect samples, i.e., $N_{tx} = N_f$. Comparing the $\mu_{t_{\%}}$ curves to the corresponding reconstruction performance metrics we see that as the $t_{\%}$-average mutual coherence is lowered, the reconstruction quality improves. Regular sampling introduces signal aliasing manifested as periodic and large column cross-correlation peaks that confuse the reconstruction algorithm. The $t_{\%}$-average mutual coherence is the lowest when $\mathbf{k}$-space sampling points cover the available $\mathbf{k}$-space extent most uniformly. The most uniform coverage in the regular subsampling case is achieved when the ratio of the number of aspect angles to the number of frequency samples is approximately $N_{tx}/N_f = \Delta K_x/\Delta K_y$, where ΔK_x (ΔK_y) is the $\mathbf{k}$-space extent in the cross-range (range) direction. On the other hand, in the random sampling case, the $\mathbf{k}$-space coverage becomes more uniform as the number of transmitted probes increases. This is reflected in the lower values of the $\mu_{t_{\%}}$. We see that increasing the number of transmitted probes after a certain value of $\mu_{t_{\%}}$ is reached has only a small impact on the reconstruction performance. Finally, the monostatic random sensing enables high-quality reconstructions with a smaller number of probes ($N_{tx} \geq 25$) than required by the conventional, SAR Nyquist sampling

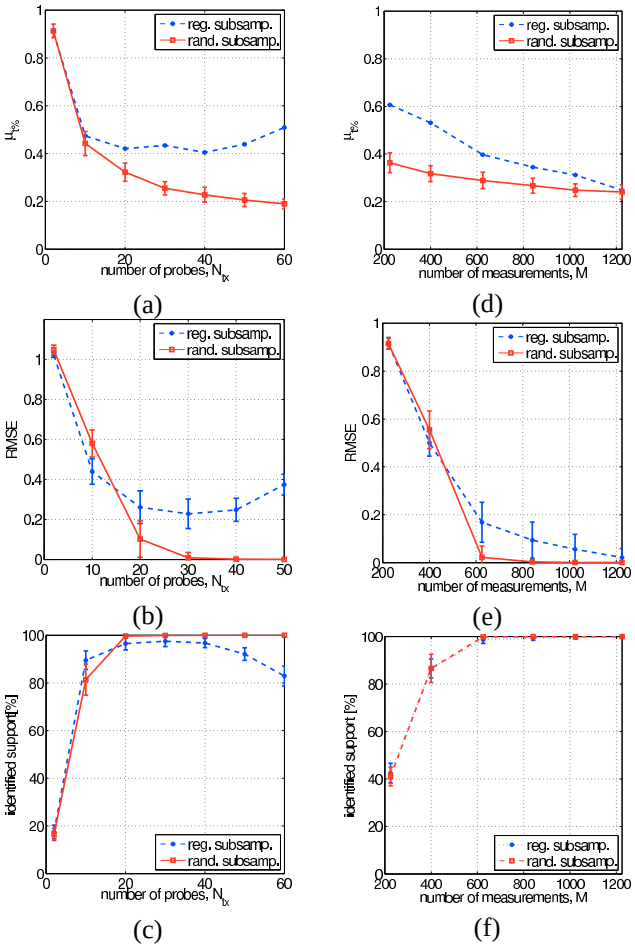

Fig. 3. Monostatic SAR when the ground scene consists of $T = 140$ scatterers. (a), (b), (c) Performance vs. sensing configuration for the fixed number of measurements $M = 600$. (d), (e), (f) Performance vs. number of measurements M for sensing configurations with $N_{tx} = N_f$. (a), (d) The $t_{\%}$-average mutual coherence, $\mu_{0.5\%}$. (b), (e) RMSE. (c), (f) Percentage of correctly identified support of T largest estimated signal peaks.

where $N_{tx} = 40$. In the right column, we observe the number of measurements needed for accurate reconstruction is 4-5 times the number of scatterers in a scene.

2) Simulation results for multistatic CS SAR: The main advantage of compressed sensing in the monostatic scenario is the reduction of data storage and reduction in the number of transmitted probes. Data collection time can not be reduced, as the monostatic SAR platform covers the whole aspect range sequentially in time. On the other hand, multistatic SAR has the potential to further reduce the data acquisition time through the use of a multitude of spatially dispersed transmitters and receivers. Theoretically, there exist many multistatic geometries with similar $\mathbf{k}$-space coverage as in the monostatic case, and thus, similar reconstruction results in the case of isotropic scattering. In an extreme case, we consider ultra-narrowband circular multistatic configurations with $N_f = 1$ and transmitters and receivers placed around the scene in a full circle [16].

In order to carry out simulations comparable to the monostatic case presented earlier, the carrier wavelength is reduced, such that spatial resolutions of the two configurations are approximately the same. In our simulations, each transmit-

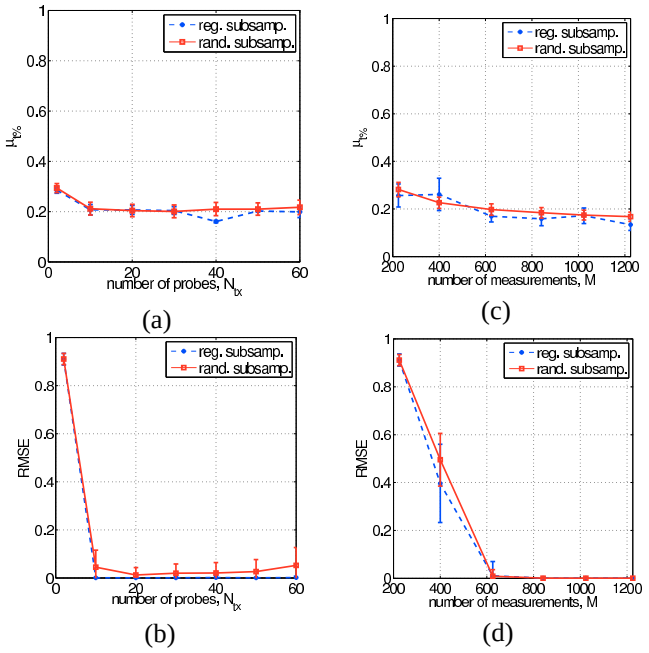

Fig. 4. Multistatic ultra-narrowband SAR when the ground scenes consists of $T = 140$ scatteres. (a), (b) Performance vs. sensing configuration for the fixed number of measurements $M = 600$. (d), (e) Performance vs. number of measurements M for sensing configurations with $N_{tx} = N_{rx}$. (a), (c) The $t_{\%}$-average mutual coherence, $\mu_{0.5\%}$. (b), (d) RMSE.

ter sends out an ultra-narrow band waveform signal with a frequency that satisfies $\rho_x = \rho_y = 0.25 = \sqrt{2}/4 \cdot c/f_o$. The scene size is the same as in the monostatic simulation cases. We assume that the isotropic scattering assumption is valid for the circular multistatic configuration.

In the left column of Fig. 4 we show results as a function of the number of spatially dispersed transmiters N_{tx} when the total number of measurements is held fixed to $M = 600 = N_{tx}N_{rx}N_f$. In the right column of Fig. 4, we show the results as a function of the number of measurements M for sensing configurations with $N_{tx} = N_{rx}$. In both cases, the signal support size is $T = 140$. All sampling cases result in a **k**-space pattern that deviates significantly from a regular **k**-grid. This translates into significantly reduced coherence of configurations with a few transmitted probes and higher-reconstruction quality as compared to the monostatic case with the same number of transmitted probes. Furthermore, different multistatic sampling patterns achieve similar performance. While the random sampling was the key to the improved performance in the monostatic case, the circular multistatic configuration is robust to transmit/receive sensor aspects. Similarly to the monostatic case the number of required measurements needed for accurate reconstruction is 4-5 times the number of scatterers in a scene.

V. Conclusion

In this paper we studied different monostatic and multistatic SAR measurement configurations in the context of compressed sensing. Compressed sensing techniques when applied to SAR allow for reliable sparsity-driven imaging with dramatically reduced number of transmitted probes. The image quality of the sparse reconstruction is primarily determined by the sampling pattern in the spatial-frequency domain. We showed that reconstructions of similar quality can be obtained using either the wide-band monostatic or ultra-narrow band multistatic configurations, effectively trading off frequency for geometric diversity. In both cases, configurations with sufficiently small values of the $t_{\%}$-average mutual coherence achieve high-quality reconstruction performance. The $t_{\%}$-average mutual coherence is an easily computed parameter that can be used in the real time design or evaluation of sensing configurations for e.g. task planning of multi-mode radars. In the multistatic case, it is straightforward to obtain low coherence either by regular or random transmit/receive aspect sampling, whereas in the monostatic case randomness in the sampling pattern leads to lower coherence. In the monostatic case, compressed sensing and sparsity-driven reconstruction allow for reduced on-board data storage and sensing with a reduced number of transmitted probes relative to what is conventionally required. In the multistatic case, compressed sensing and sparsity-driven reconstruction allow for sensing with fewer transmitted probes, but also reduced acquisition time when compared to the monostatic case.

References

[1] D. L. Donoho, "Compressed sensing," *IEEE Trans. Inform. Theory*, vol. 52(4), pp. 1289–1306, 2006.

[2] E. J. Candes, J. Romberg, and T. Tao, "Robust uncertainty principles:Exact signal reconstruction from highly incomplete frequency information," *IEEE Trans. Inform. Theory*, vol. 52(2), pp. 489–509, 2006.

[3] E. Candes and J. Romberg, "Sparsity and incoherence in compressive sampling," *Inverse Problems*, vol. 23(3), pp. 969–985, 2007.

[4] D. Donoho and X. Huo, "Uncertainty principles and ideal atomic decomposition," *IEEE Trans. Inform. Theory*, vol. 47, no. 7, pp. 2845–2862, 2001.

[5] M. Lustig, D. Donoho, and J. M. Pauly, "Sparse MRI: The application of compressed sensing for rapid MR imaging," *Magnetic Resonance in Medicine*, vol. 9999, 2007.

[6] C. V. Jakowatz, D. E. Wahl, P. S. Eichel, D. C. Ghiglian, and P. A. Thompson, *Spotlight-mode Synthetic Aperture Radar: a Signal Processing Approach*. Norwell, MA: Kluwer Academic Publishers, 1996.

[7] M. Cetin, *Feature-Enhanced Synthetic Aperture Radar Imaging*. Boston University: Ph.D. Thesis, 2001.

[8] M. A. Herman and T. Strohmer, "High-resolution radar via compressed sensing," *IEEE Trans. Signal Processing*, vol. 57, no. 6, pp. 2275 – 2284, 2009.

[9] Y.-S. Yoon and M. G. Amin, "Compressed sensing technique for high-resolution radar imaging," *Signal Processing, Sensor Fusion, and Target Recognition XVII, SPIE*, vol. 6968, no. 1, 2008.

[10] R. Baraniuk and P. Steeghs, "Compressive radar imaging," *IEEE Radar Conference*, pp. 128–133, 2007.

[11] S. Bhattacharya, T. Blumensath, B. Mulgrew, and M. Davies, "Fast encoding of synthetic aperture radar raw data using compressed sensing," *IEEE 14th Workshop on Statistical Signal Proc.*, pp. 448–452, 2007.

[12] I. Stojanovic, W. C. Karl, and M. Cetin, "Compressed sensing of mono-static and multi-static SAR," in *Compressed sensing of mono-static and multi-static SAR*, E. G. Zelnio and F. D. Garber, Eds., vol. 7337. SPIE, 2009, p. 733705.

[13] V. Patel, G. Easley, D. Healy, and R. Chellappa, "Compressed synthetic aperture radar," *IEEE Journal of Selected Topics in Signal Processing*, vol. 4, no. 2, pp. 244 –254, april 2010.

[14] E. van den Berg and M. P. Friedlander, "SPGL1: A solver for large-scale sparse reconstruction," June 2007, http://www.cs.ubc.ca/labs/scl/spgl1.

[15] M. Elad, "Optimized projections for compressed sensing," *IEEE Trans. Signal Processing*, vol. 55, no. 12, pp. 5695–5702, 2007.

[16] B. Himed, H. Bascom, J. Clancy, and M. C. Wicks, "Tomography of moving targets (TMT)," in *Sensors, Systems, and Next-Generation Satellites*, H. Fujisada, J. B. Lurie, and K. Weber, Eds., vol. 4540, no. 1. Proc. SPIE, 2001, pp. 608–619.